

**Transient Light-Scattering State in a Glassy  
Ferroelectric Nematic Liquid Crystal**

by

**MENGJIE CHEN**

Department of Physics

*Thesis Adviser:*

Noel A. Clark | Department of Physics

Committee members:

*Honors Council Representative:*

Paul Beale | Department of Physics

*Outside Reader:*

David M. Walba | Department of Chemistry

University of Colorado Boulder

April 4th, 2023

## Abstract

Ferroelectric nematic phase ( $N_F$ ) is a recently discovered fluid state that occurs at temperature below conventional nematic state [1]. Such a state has been expected since 1916 when predicted first by Max Born, but its existence has only been demonstrated by experiments in a synthesized material RM734 in 2020. The macroscopic polarization and the three-dimensional homogenous fluidity of such a state promise it novel electric-optical responses. To understand this new phase further, we doped RM734 with a strong red dye (DR1) and characterized this mixture. During the characterization of the mixture, a transient light-scattering state was observed in this mixture at room temperature after quenching. This unique electric-optic response was first seen in this NF phase and a detailed study on its dynamics is done.

**Keywords:** Liquid Crystals (LCs), ferroelectric nematic ( $N_F$ ), RM734, DR1, mixture, glassy ferroelectric nematic ( $N_F^G$ ), surface orientation, light-scattering, domain wall.

## Acknowledgements

I would like to thank all the people who provided me supports for my work and life  
at the University of Colorado Boulder

Professor Noel A. Clark, Dr. Xi Chen

Professor Joseph MacLennan

Dr. Cheol Park

Professor Matthew Glaser

Professor David M. Walba

Carter Bennett, Blake Maly, Ravin Chowdhury, Keith G Hedlund

Annett Baumgartner

*University of Colorado Boulder and Soft Materials Research Group*

Professor John Cumalat, Professor Jun Ye, Professor Paul Beale, Professor Michael

Ritzwoller

Kristen Apodaca

*University of Colorado Boulder*

And my friends and family

## CONTENTS

### CHAPTER 1 Background

INTRODUCTION .....	1
1.1 Background .....	3
1.1.1 Thermotropic Liquid Crystals (LCs) phases.....	3
1.1.2 Structure of nematic .....	3
1.1.3 Birefringence.....	5
1.1.4 Paraelectricity and Ferroelectricity .....	7
1.1.5 LC Cell and Surface Alignment.....	8

### CHAPTER 2 Previous study on Ferroelectric Nematic (NF) Phase

2.1 First Principles Demonstration of $N_F$ Phase.....	9
2.2 Surface orientation of NF phase: Polar Monodomains and Twisted State.....	10

### CHAPTER 3 Experiments Setup

3.1 Introduction .....	13
3.2 Preparation the sample .....	13
3.3 Depolarized Transmitted Light Microscopy (DTLM)...	15

3.4 He-Ne Laser Setup.....	16
CHAPTER 4	
Experiment results	
4.1 Introduction .....	18
4.2 Glassy Ferroelectric nematic state (NFG) and Light-scattering state .....	18
4.3 Formation and Annealing of Transient Light Scattering State .....	22
4.4 Intensity measurements using He-Ne Laser.....	26
4.5 Transient Light Scattering State Observed in other NF with no Dye .....	27
CHAPTER 5	
Discussions	
5.1 Dependence of the Reversal Dynamics on Temperature . .....	30
5.2 Dependence of the Reversal Dynamics on Field Strength .....	30
5.3 Model.....	31
CHAPTER 6	
Conclusion .....	33
REFERENCES .....	34
APPENDIX	
I    MATLAB code for intensity scan .....	35

## FIGURES

### Figure

1.1	Common LC phases.....	4
1.2	Schematic illustration of indicatrix of a uniaxial material .....	6
1.3	Macroscopic schematic illustration of N phase in contact with a solid substrate .....	8
2.1	Simplified illustration of N phase and N <sub>F</sub> phase .....	9
2.2	Polarization density of RM734 vs. temperature .....	10
2.3	Cell structures of NF phase in RM734 under different alignments .....	12
3.1	Cell geometry.....	14
3.2	Schematic setup of a polarizing microscope.....	15
3.3	Optical path diagram of He-Ne laser setup.....	17
4.1	Phase diagram of the mixture of 5 wt.% DR1 and 95 wt.% RM734 under slow cooling.....	18
4.2	DTLM images of RM734 dopes with DR1 (5 wt.%).....	19
4.3	Dynamics of scattering state under crossed polarizer and analyzer .....	20
4.4	Transient scattering state.....	21
4.5	Evolution of the scattering state in a planar-aligned cell of doped RM734 in the NF phase (t = 8 μm) .....	22

4.6	Transmitted intensity across the electrode gap after field reversal	24
4.7	Optical signal of transmitted laser beam detected by photodetector	26
4.8	Mixture of DIO and RM734	28
5.1	Time durations of processes of the scattering state at different temperatures	29
5.2	Polarization reorientation response to applied E field	32

## CHAPTER 1 Background

### INTRODUCTION

The recently discovered ferroelectric nematic phase ( $N_F$ ) phase exhibits fast polar switching and unique electro-optic response due to its large macroscopic polarization  $\sim 6\mu C/cm^2$  [1]. In the experiment, we discovered that by quenching the  $N_F$  rapidly to room temperature, and glassy ferroelectric nematic phase is achieved ( $N_F^G$ ). In the pure ferroelectric nematic material RM734, due to the monotropic nature of the  $N_F$  phase, the glassy ferroelectric phase ( $N_F^G$ ) could live for several hours before crystal gradually grows into the phase. In general, past studies show that doping pure material with other molecules would suppress the crystallization. In this research, we mix RM734 with dye DR1 and achieve a more stable  $N_F^G$  phase which could live for days. The  $N_F^G$  phase, despite its huge viscosity, still shows polar switching behaviors. As explained in Figure 2 and 3, application of an DC electric field with strength  $0.1 V/\mu m$  would slowly align the director into a uniform state in 10 minutes. Upon the field reversal, instead of homogenous reorientation of polarization, we observed a unique transient scattering state which appears dark with or without analyzer. The scattering cross section appears to be largely isotropic and shows little dependence on the incident and scattered polarization. The scattering state would gradually disappear if one reverses the sign of field to the initial orientation for 10 mins (Fig. 4.3), or keep applying the reversal field for

another 1 hour (Fig. 4.5). A similar phenomenon was observed by Joseph E. MacLennan and Noel A Clark in the ferroelectric smectic C material DOBAMBC, using stroboscopic microscopy [2]. In this research, the detailed dynamic of the formation and disappearance of the said scattering state is studied and demonstrated, thanks to extremely slow switching due to the enormous viscosity. The uniform state  $\rightarrow$  scattering state  $\rightarrow$  uniform state switching in the  $N_F^G$  state exhibits a different optic switching mode, the transient scattering mode, from the reported homogenous reorientation mode and soliton dominated mode [3]. It is interesting to see whether the transient scattering mode could be reproduced in the fluid  $N_F$  phase in future study. From the application perspective, the scattering nature of the transient state has a potential in optical switch applications, such as smart window, where the uniform state is the “on” state and the scattering state is the “off” state. The isotropic scattering makes it possible to make devices without traditional analyzer and polarizer, which increases the potential maximum on-state transmission efficiency from 50% to 100% and also reduces the manufacture cost. Compared to devices based on absorption, devices based on scattering may be more easily temperature controlled. In this study, the material is made of a mixture of ferroelectric nematic material RM734 and dye DR1, so both scatter and absorption effects are present. The same scattering state could be observed in the quenched RM734 sample, even though it is less stable. In principle, the dye dopant is not necessary, any material mixed well with ferroelectric is a candidate for the stable

$N_F^G$  phase. However, in this study, the dye absorption increases the contrast between the scattering state and the uniform aligned states.

## 1.1 Background

This section introduces the basic physics on liquid crystals that help to explain the experimental methods and results in the project.

### 1.1.1 Thermotropic Liquid Crystals (LCs) phases

Liquid crystals (LCs) are partially ordered fluids that are thermodynamically stable between solid crystals and isotropic liquids [4]. Within LCs, they are further classified into different phase types based on the symmetry breaking in contrast to isotropic state [5]. Applying certain conditions can induce phase transitions of LCs where different phases correspond to different states of LCs behave in distinct ways. Based on the conditions at which LC have different phases, they can be divided into two types of LC: lyotropic and thermotropic. Lyotropic LC can have phase transition induced from change in concentration while thermotropic LC have different phases at different temperatures. All the LCs used in this project belong to thermotropic LCs.

The most common phases of LC are crystal, smectic, nematic and isotropic phase (Fig 1.1). In crystal phase, molecules form a well-structured crystalline lattice. They stay in fixed positions and can only vibrate to a limited extent. After heating, we can achieve smectic phases where molecules can move freely within structured layers. Further heating the sample can lead to nematic phase where structured layers in smectic phases are removed. Molecules now can move like a fluid but they still have an average orientation indicated by  $\mathbf{n}$  director. In isotropic

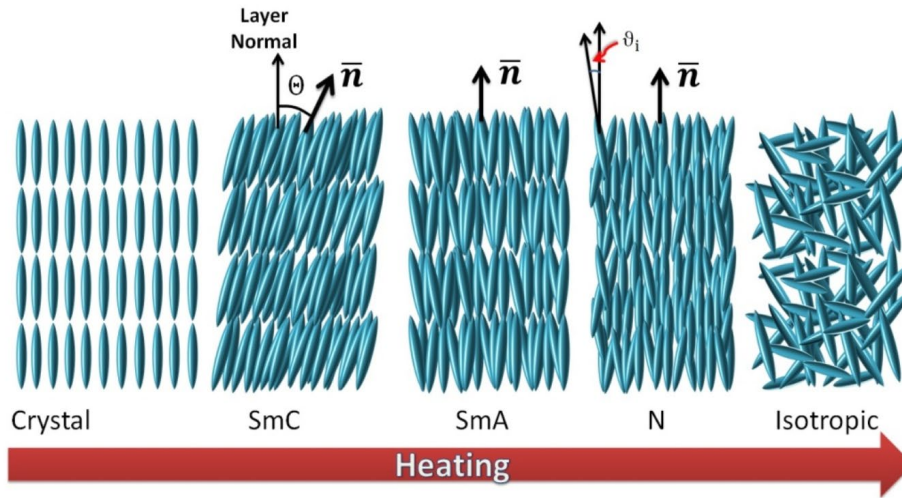


Fig 1.1 Common LC phases seen after heating from crystalline state. Rod-like shapes are the LC molecules. In crystal phase, molecules are aligned in a well-structured lattice. After heating, smectic phases, SmC and SmA, are achieved where molecules can move around within smectic layers. The director  $\mathbf{n}$  denotes the average orientation of the molecules. In SmA,  $\mathbf{n}$  is parallel to the layer normal while in SmC,  $\mathbf{n}$  is tilted. Further heating induces to nematic phase (N) where molecules can move freely in all directions without layers. In isotropic phase, molecules can move freely and there is no preferred average orientation. (Figure adapted from [3])

phase, LC behaves just like any other liquid. Molecules can move freely and there is no preferred average orientation of molecules.

### 1.1.2 Structure of the Regular Nematic (N) phase

In this section, terminology and basics on N phase are introduced to better understand the project.

There are two types of nematic phases, regular nematic N and cholesteric nematic  $N^*$  phase. In regular nematic phase the centers of mass of molecules are distributed randomly, there is no translational order. However, there is orientational order as molecules tend to align themselves with same direction [6].

Such an order is long range as molecules tend to have the same average orientation at equilibrium regardless of the size of the sample. This average orientation is denoted by director  $\mathbf{n}$ , which may be treated as a vector. To describe how well the individual molecular long axes are ordered in a convenient way, order parameter  $S$  was invented [5]:

$$S = \frac{1}{2} \langle 3 \cos^2 \theta - 1 \rangle \quad (1)$$

$\theta =$  the angle between the molecular long axis and the director  $n$ (fig 1.1).  
the  $\langle \rangle$  brackets denote stastical averaging.

An order parameter should be zero in a disordered structure and nonzero in an ordered structure [7], for example,  $S$  is zero in isotropic phase, one in solid crystals, and it decreases from smectic to N phases.

### 1.1.3 Birefringence

To study the textures of uniaxial liquid crystal phases such as N and SmA, and retrieve dynamics of molecules, birefringence is an important concept to understand.

Birefringence happens when the refractive index parallel  $n_{||}$  to the optical axis is different from that perpendicular to the axis  $n_{\perp}$ . The optical axis is the normal to the plane whose cut with indicatrix is a circle (Fig. 1.2.). The indicatrix is an ellipsoid with its long and short axes parallel and perpendicular respectively to the optical axis for optically positive medium (Fig. 1.2. A), the opposite happens for optically negative medium (Fig. 1.2. B). In our material,  $n_{||}$  is greater than  $n_{\perp}$  as shown in Fig 1.2 (A).

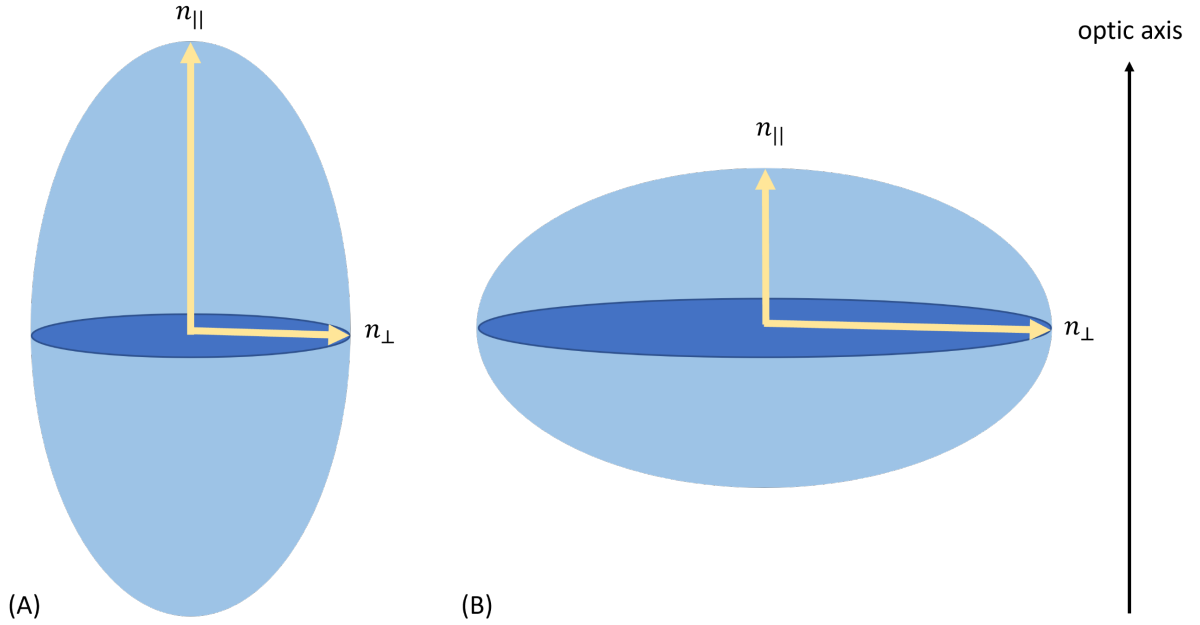


Fig. 1.2. Schematic illustration of indicatrix of a uniaxial material. (A) Indicatrix of optically positive medium,  $n_{||}$  is parallel to optic axis and  $n_{\perp}$  is perpendicular to the optic axis. (B) Indicatrix of an optically negative medium,  $n_{\perp}$  is parallel to optic axis and  $n_{||}$  is perpendicular to the optic axis.

A traveling light beam can be split into ordinary ray and extraordinary ray where ordinary ray follows Snell's law of refraction and extraordinary ray does not [8]. Their polarizations are perpendicular to each other and experience different refractive index  $n_o$  and  $n_e$  when propagating through a birefringent medium. The phase difference  $\delta$  resulted is given by,

$$\delta = \frac{2\pi}{\lambda} (n_e - n_o) d \quad (2)$$

$\lambda = \text{wavelength in vacuum}; d = \text{distance traveled in medium};$

The  $n_o$  and  $n_e$  are related to the  $n_{||}$  and  $n_{\perp}$  by the following equations [8],

$$n_o = n_{\perp} \quad (4)$$

$$n_e = \frac{n_{||} n_{\perp}}{\sqrt{n_{||}^2 \cos^2 \phi + n_{\perp}^2 \sin^2 \phi}} \quad (5)$$

$\phi$  = the angle between the optic axis and the direction of light propagation.

Therefore, if there is light polarized by a linear polarizer propagated through a birefringent medium such as N phase, this transmitted linearly polarized light becomes elliptically polarized and a portion of it can pass through a second polarizer (analyzer) placed at right angles to the first polarizer. On the other hand, if the material is isotropic, all the light will be blocked by the crossed analyzer and polarizer. This is going to be the foundation for the analysis of observations in the project presented later.

#### 1.1.4 Paraelectricity and Ferroelectricity

Most molecules building up liquid crystals are polar, i.e., the dipole moment of the individual molecule is non-zero. However, the nematic phase built up of these polar molecules are macroscopic non-polar. This means that the director  $\mathbf{n}$  is not polar, i.e., physical properties are the same flipping  $\mathbf{n}$  to  $-\mathbf{n}$  in nematic phase [7]. Although there is no permanent polarization, nematic phase can have induced polarization from applying external electric field  $\mathbf{E}$ . Materials that can have induced polarization through applying electric field are said to be paraelectric. When  $\mathbf{E}$  is turned off, the polarization  $\mathbf{P}$  also returns to zero. When a non-zero  $\mathbf{E}$  is applied, positive and negative charges in regular nematic molecules are pulled apart inducing a temporary  $\mathbf{P}$ . The induced  $\mathbf{P}$  resulting molecules experiencing torque from the applied  $\mathbf{E}$  and reorient to align with  $\mathbf{E}$ . When the direction of  $\mathbf{E}$  is reversed, induced polarization also inverses its direction so molecules do not reorient.

On the other hand, ferroelectric materials have a permanent non-zero polarization  $\mathbf{P}$  usually much larger than the induced polarization. Due to this non-zero permanent  $\mathbf{P}$ , molecules align with applied E-field and reorient when direction of E-field is reversed. The term “ferroelectric” is an analogy to “ferromagnetic” as ferroelectric materials tend to respond to an applied electric field in an analogous manner ferromagnets respond to a magnetic field.

### 1.1.5 LC Cell and Surface Alignment

To study the texture of nematic liquid crystals, samples are filled into a thin glass cell before investigating under microscope. A cell usually consists of two glass slides and the sample goes into the thin space between them. In addition, treatment can be done on the surface of these glass slides to orient liquid crystals. The physics behind it is that when a N phase is placed in contact with solid, a bounding surface is created [9]. This surface perturbs the nematic order close to it as shown in Fig. 1.3.



Fig. 1.3. Macroscopic schematic illustration of N phase in contact with a solid substrate. The arrows stand for the apolar director  $\mathbf{n}$  in the bulk.

## Chapter 2

### Previous study on Ferroelectric Nematic ( $N_F$ ) Phase

This chapter presents the two major recent studies conducted regarding the ferroelectric nematic ( $N_F$ ) phase. These two studies demonstrate the evidence of the existence of  $N_F$  phase and present electro-optic effects of  $N_F$  phase under different surface alignments.

#### 2.1 First Principles Demonstration of $N_F$ Phase

In 2020, Chen et al published a paper presenting the first evidence of the existence of  $N_F$  phase [1]. The material being studied is calamitic compound 4-[(4-nitrophenoxy)carbonyl]phenyl-2,3-dimethoxybenzoate (RM734). The difference

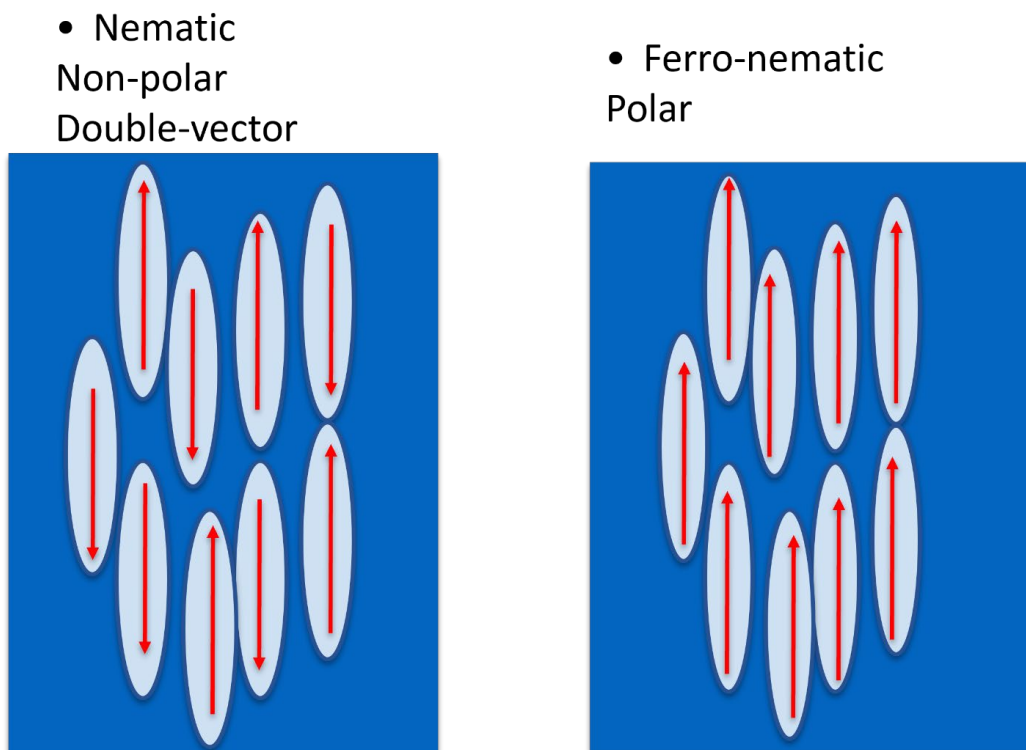


Fig. 2.1 Simplified illustration of N phase (left) and  $N_F$  phase (right). Rod-like shapes are the LC molecules. Red arrows show the direction of dipole moment of each molecule.

between this  $N_F$  and regular nematic phase can be illustrated using Fig. 2.1. In N phase there is no macroscopic polarization although each molecule is polar. They align themselves such that the molecules with dipole moment pointing up are

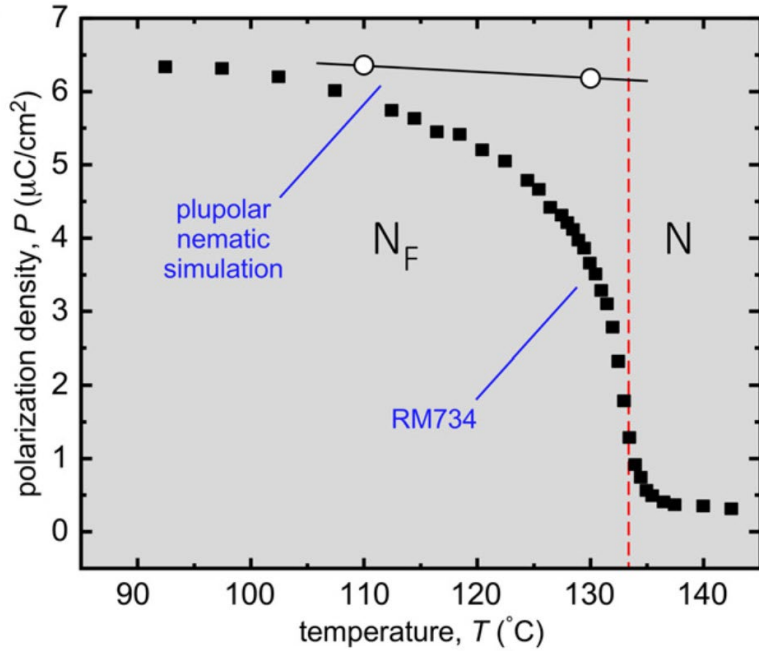


Fig. 2.2 Polarization density of RM734 vs. temperature. (Figure adapted from Chen et al. [1])

distributed evenly with those having dipole moment pointing down. The overall polarization is zero as microscopic polarizations of the molecules cancel out with each other. In  $N_F$  phase, however, the molecules align themselves such that the dipole moments of the polar molecules all point in the same direction resulting in a large macroscopic polarization. The macroscopic polarization density of  $N_F$  phase in RM734 was measured to be as big as  $\sim 6 \mu\text{C}/\text{cm}^2$  (Fig.2.2).

## 2.2 Surface orientation of $N_F$ phase: Polar Monodomains and Twisted State

As mentioned in section 1.2.2, a substrate, after certain treatments such as buffing, exerts perturbations on molecules in fluid-like N phase close to it. In  $N_F$  phase, molecules close to the surface also orient with their director along the buffing

direction on the substrate. There is a difference though due to the additional polar order of  $N_F$  phase. In  $N$  phase,  $\mathbf{n}$  to  $-\mathbf{n}$  is a symmetric operation, i.e., the physical properties remain the same after the operation. This is not the case in  $N_F$  phase because the macroscopic polarization adds a polar order parameter. This results in the molecules not only orientating along the buffing direction, but also having their polarization reorienting to a certain direction when the buffing is unidirectional instead of bidirectional [3]. Unlike  $N$  phase where molecules have a quadrupolar surface interaction and therefore behave the same in bidirectional buffing and unidirectional buffing.

The surface with bidirectional buffing is nonpolar, and the one with unidirectional buffing is polar as shown in Fig. 2.3. When the cell is cooled to lower temperature, transition from  $N$  to  $N_F$  happens and the polarization parameter of molecules becomes polar. In the case of bidirectional buffing, they form uniform polar  $N_F$  domains in either direction of the buffing (Fig. 2.3 A, C). In the case of antipolar cells with unidirectional buffing, transition of  $N$  to  $N_F$  first induces a polar monodomain of  $N_F$  in Fig.2.3 B. However, there is a mismatch of polarization on the warmer surface. Upon further cooling, there will be a spontaneous surface transition on the warmer plate, forming a  $\pi$  twist state as illustrated in (Fig. 2.3 E). There could be two types of  $\pi$  twist states with opposite chirality separated by a  $2\pi$  domain wall (Fig. 2.3 D)

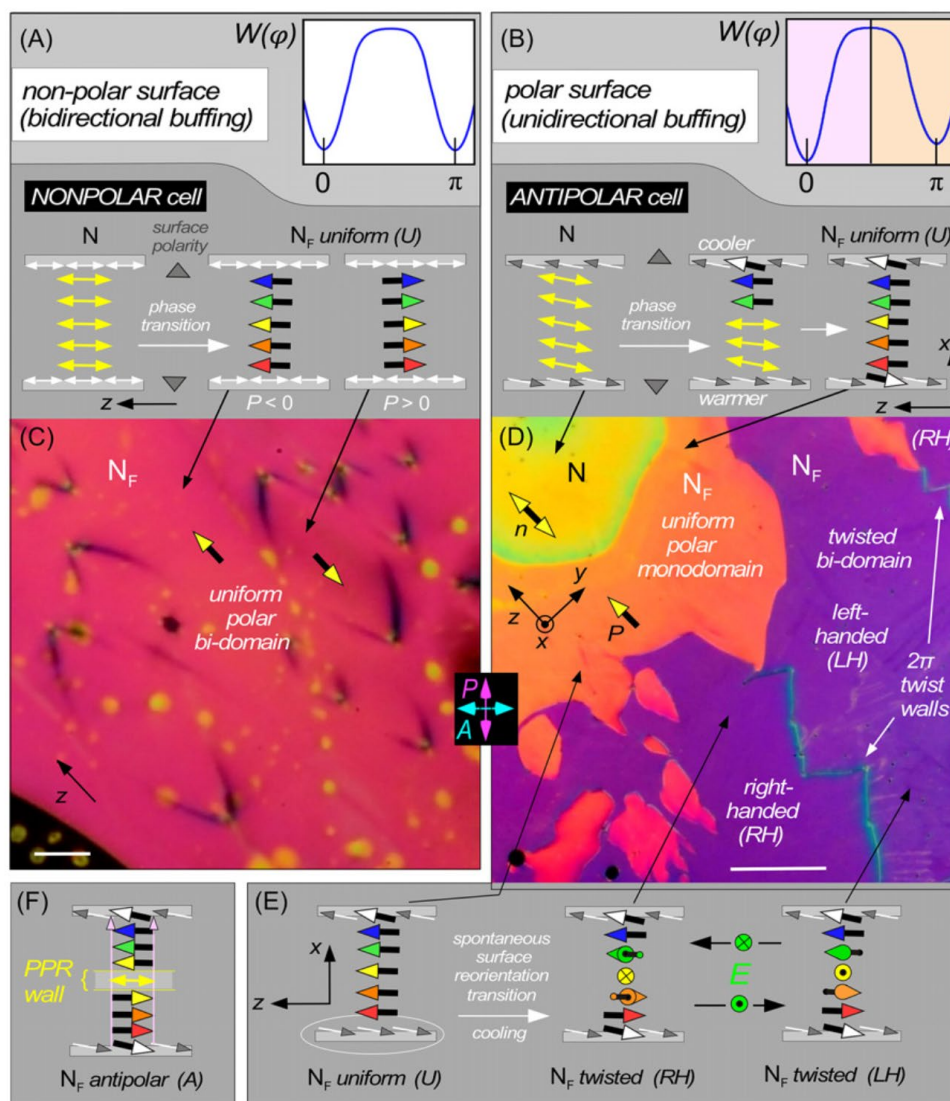


Fig. 2.3. Cell structures of  $N_F$  phase in RM734 under different alignments obtained from Chen et al. [9]. (A,C) the schematic illustration and DTLM images of orientation of molecules in N and  $N_F$  phase in nonpolar cell. In N phase, the director is bipolar. In nonpolar surface,  $N_F$  can form uniform domain in both directions. (B,D and E) the schematic illustration and DTLM images of orientation of molecules in N and  $N_F$  phase in antipolar cell. The buffing above and below is unidirectional and antiparallel. In N phase, molecules align along the buffing direction just like in nonpolar cell. Orange  $N_F$  uniform polar monodomain is formed in (D). The cell cooled with a temperature gradient induces transition of orientation of warmer molecules to twisted  $N_F$  as shown in (E). (F) The cell cooled homogeneously has structure of antipolar, uniform director state with pure polarization reversal wall between domains with opposite orientations. (Scale bar: C, 20  $\mu\text{m}$ ; D, 200  $\mu\text{m}$ .)

## Chapter 3

### Experiments Setup

#### 3.1 Introduction

Based on the previous studies on  $N_F$  phase, we hypothesized that there will be other electrooptic effects of the mixture of  $N_F$  phase. We doped RM734 with a strong red dye and characterized the doped mixture first under DTLM and then probed using He-Ne laser.

#### 3.2 Preparation of the Sample

5 wt.% DR1 (Sigma-Aldrich) and 95 wt.% RM734 were weighed using electronic balance and transferred to a glass vial. The bottle was then heated up to 190°C for 5 mins until RM734 is in the isotropic phase, the sample was then thoroughly mixed with stir bar. An empty liquid crystal cell was heated in advance on a heating bench at 180°C before filled with mixture. The filled cell was then quenched to room temperature by taking it off the heating bench and cooling in the air. The molecular structures of the materials and the cell are shown in Fig. 3.1. The experiment cell is purchased from INSTEC. The cell is made of two glasses spaced with an 8  $\mu\text{m}$  gap where the mixture is filled in. On bottom cell surface, two ITO electrodes are deposited with a separation of 1mm (Fig 3.1). When a voltage is applied on the electrodes, an in-plane electrode field is established. Planar rubbing alignment is applied on both surfaces, where the rubbing direction is largely parallel to the

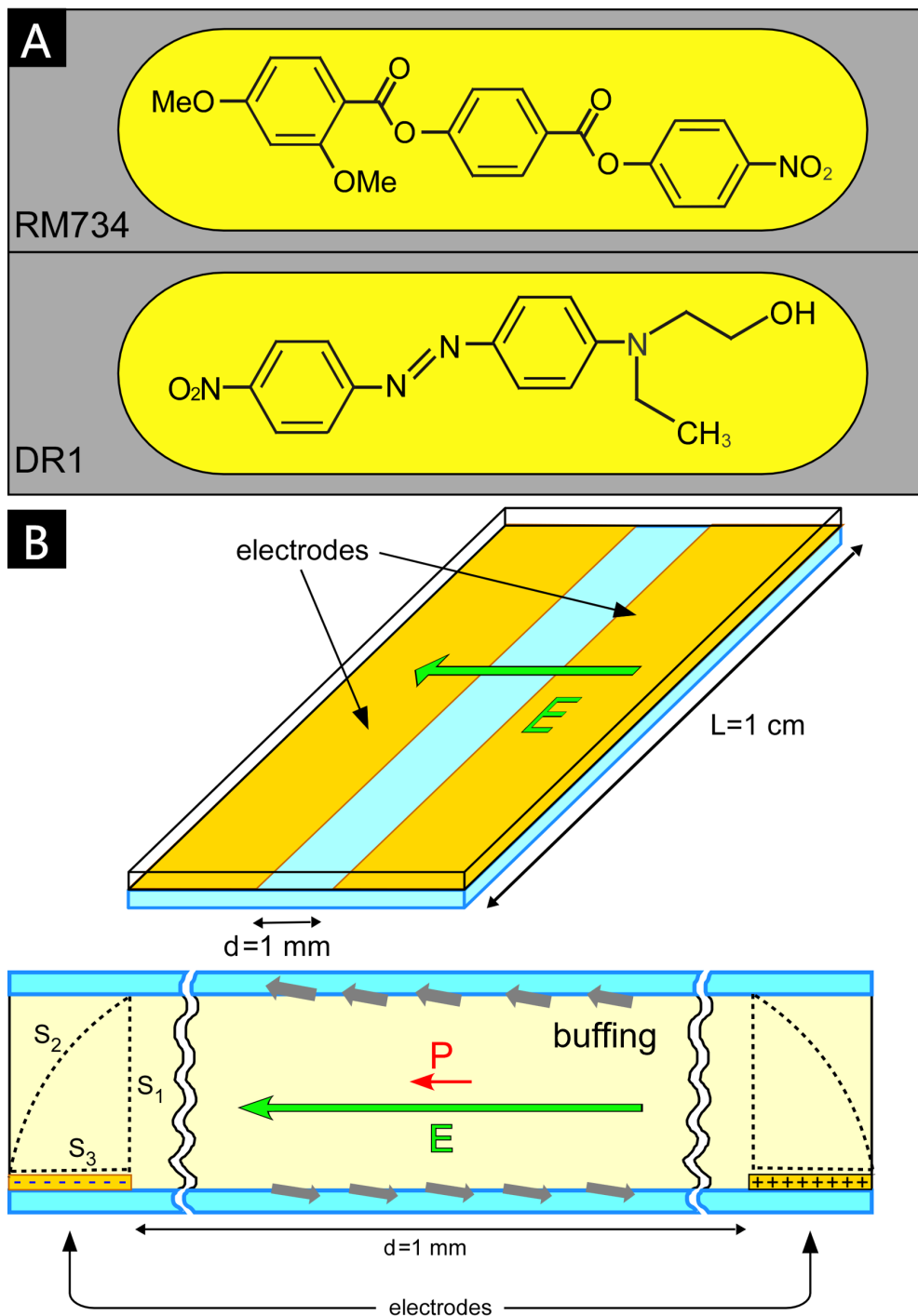


Fig. 3.1. (A) Molecular structures of RM734 and disperse red 1 (DR1). (B) Cell geometry. An in-plane field can be applied across the electrode gap.

applied field direction with a 3 deg offset. In the perspective of polar alignment, the cell exhibit antiparallel buffering which introduces a spontaneous  $\pi$  twist state in the

$N_F$  phase [3].

### 3.3 Depolarized Transmitted Light Microscopy (DTLM)

To study the textures of the cell and characterize the sample through electrooptic effects, we use depolarized transmitted light microscopy (DTLM). DTLM is a microscopy set-up commonly used in the study of liquid crystals. A typical setup of a microscope used to take DTLM images is shown in Fig. 3.2.

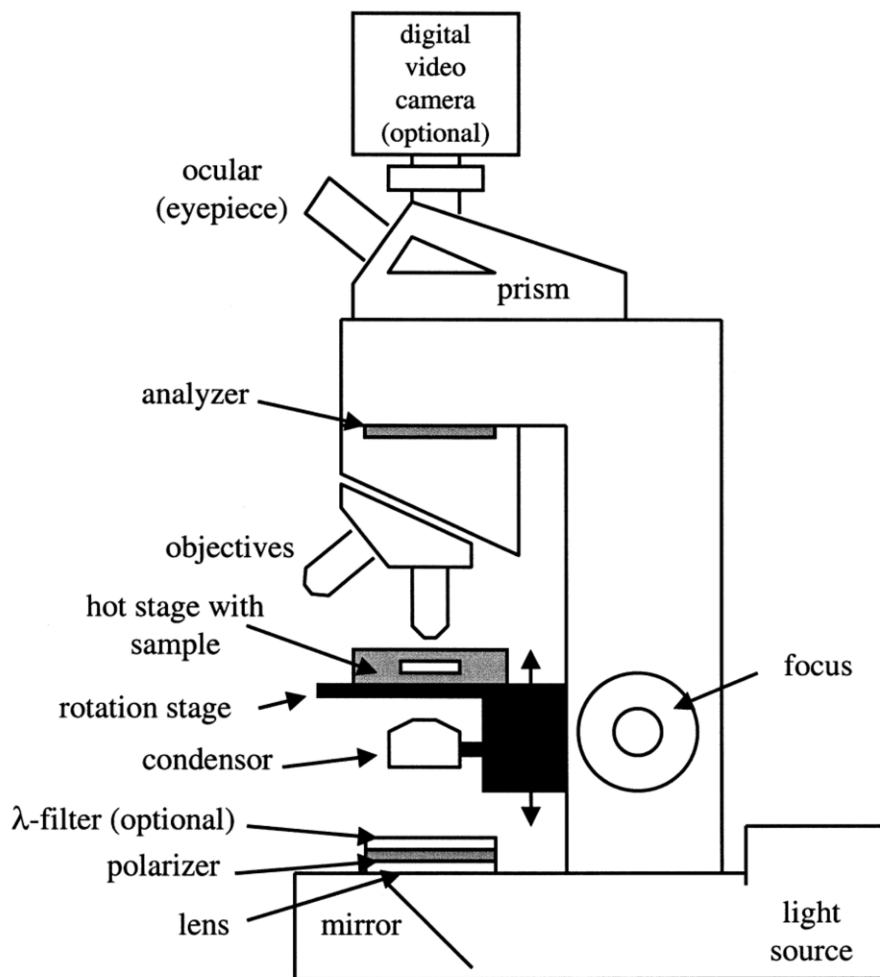


Fig. 3.2 Schematic setup of a polarizing microscope. DTLM images are taken using the digital video camera installed on top of the microscope. (Figure obtained from Dierking [7])

A white light beam is first emitted from the light source, usually a halogen light bulb [6]. The mirror reflects the light so that the light travels to eyepiece and camera all the way from the bottom. Before light reaches the eyepiece, it is first polarized by the polarizer before the condenser. The polarized light is then collected by the condenser which enables the uniform illumination of the sample. The LC sample is placed on rotation stage equipped with a hot stage connected to temperature controller that can maintain the sample at certain temperature. Polarized microscopes are usually equipped with objectives, magnification of x5, x10 and x20 are the common ones used for texture studies. In this project, magnification of x5 is used most of the time. After the objective, there is a second polarizer named analyzer that is rotatable and removable. In this project, the analyzer is oriented at right angles to the polarizer at the bottom such that it is completely black to look when no birefringent sample is inserted.

### **3.4 He-Ne Laser Setup**

Apart from qualitative observations from DTLM, quantitative data about the cell was obtained with aid of He-Ne laser set-up. He-Ne laser is ideal because it is red and the sample absorbs little red light. This laser set-up is used to collect data about the scattering state in  $N_F^G$  phase observed in the quenched cell of doped RM734. Details about the scattering state are in Chapter 4.

The optical path diagram of the He-Ne laser is shown in Fig. 3.3. A neutral density filter (ND filter) is used to reduce the intensity of the laser such that the

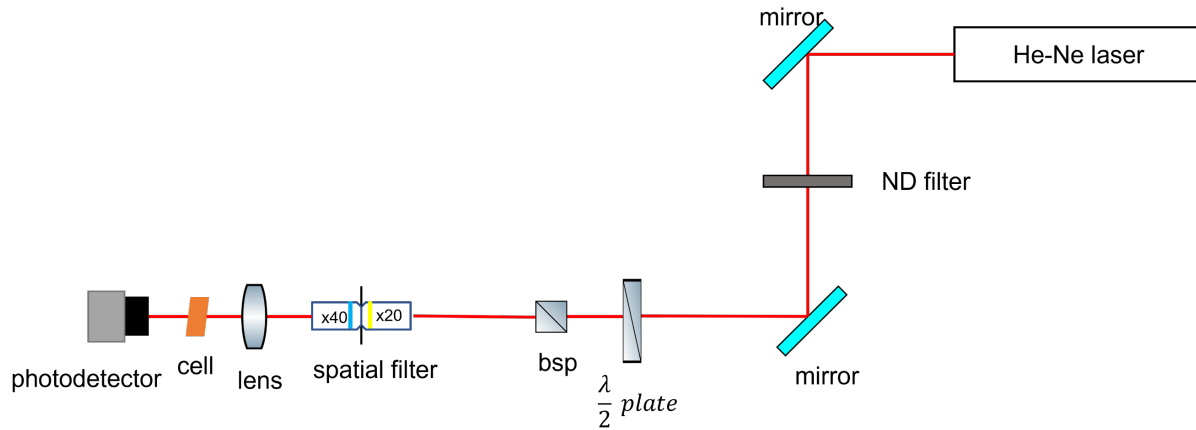


Fig. 3.3 Optical path diagram of He-Ne laser setup. A laser beam is emitted from He-Ne laser. The laser hits two optical mirrors and with a neutral density filter (ND filter) in between. The ND filter decreases the intensity of the laser. The laser then hits a half-wave plate and a beam splitter polarizer. Two objectives with a pinhole between them are placed as a spatial filter. An optical lens with focal length of 100 mm is used to focus the laser. The prepared cell of doped RM734 is placed between the lens and a photodetector.

sample in the cell is not burnt by the laser. The half-wave plate rotates the polarization of incoming laser. Intensity of the laser can be further modified by rotating the beam splitter polarizer after it. Objectives with a pinhole serve as a filter and the lens focuses the laser onto the cell. A photodetector is a photodiode used to detect the optical signal from the transmitted laser. These signals are projected onto and exported from an oscilloscope.

## Chapter 4

### Experiment Results

#### 4.1 Introduction

As described in previous section, a mixture of 5 wt.% DR1 and 95 wt.% RM734 was prepared and filled into the antiparallel rubbed (antipolar buffing) cell. This cell showed some unexpected electro-optical phenomenon at room temperature. It formed a twisted glassy ferroelectric nematic ( $N_F^G$ ) phase after quenching to 25°C. Application of DC field induces it to a uniform monodomain. Moreover, a transient light-scattering state was observed in the  $N_F^G$  phase with reversal of electric field. This chapter summarizes the experiment observations of the  $N_F^G$  phase and transient light-scattering state.

#### 4.2 Glassy Ferroelectric nematic state ( $N_F^G$ ) and Light-scattering state

The first thing to do characterizing a liquid crystal sample is to draw a phase diagram of it. To draw a phase diagram, the sample is heated up to isotropic phase and slowly cooled down while being monitored under polarized microscope such that the phase transition temperatures can be recorded. Under slow cooling, the phase diagram for the mixture of 5 wt.% DR1 and 95 wt.% RM734 is shown in Fig. 4.1.

slow cooling:  
Iso – 175°C – N – 110°C –  $N_F$  – 55°C – crystal

Fig. 4.1. Phase diagram of the mixture of 5 wt.% DR1 and 95 wt.% RM734 under slow cooling.

The sample crystallizes at temperature under  $55^{\circ}\text{C}$  with little crystals formed as shown in Fig.4.2 A. However, after quenching the cell to room temperature, the sample forms a  $\pi$  twist planar aligned state instead of crystal conglomerate as shown in Fig. 4.2. B. Moreover, this planar aligned state exhibits polar switching on the time scales of tens of minutes. Therefore, this is believed to be a glassy ferroelectric nematic phase ( $\text{N}_{\text{F}}^{\text{G}}$ ).

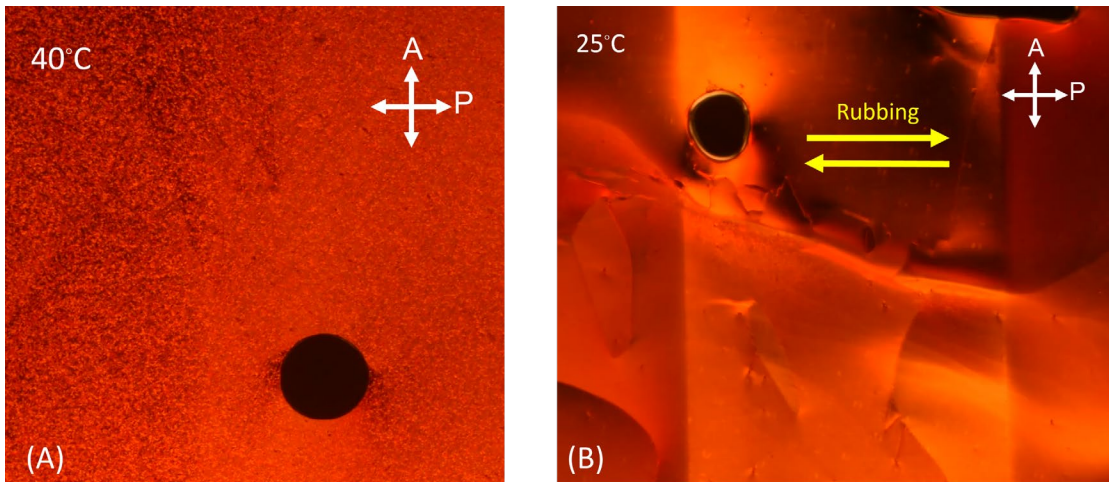
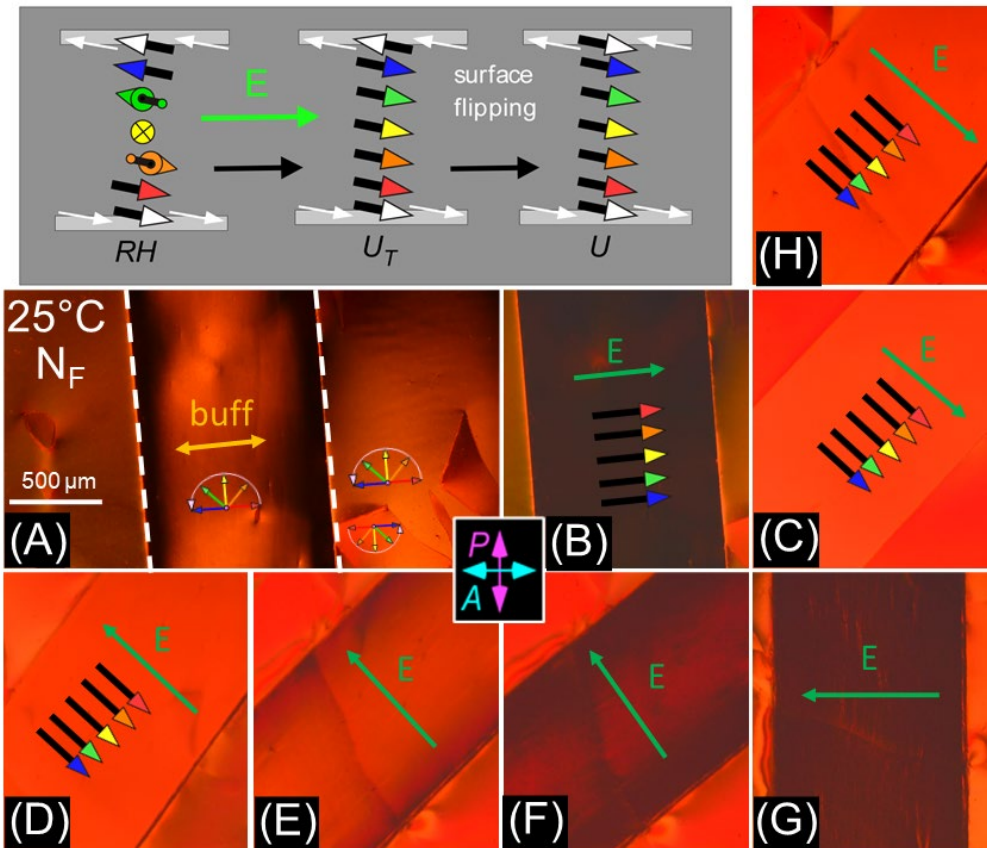


Fig.4.2 DTLM images of RM734 doped with DR1 (5 wt.%). (A) crystallized sample at  $40^{\circ}\text{C}$  after slow cooling. (B)  $\pi$  twist planar aligned state at room temperature after quenching.

Starting with the initial  $\text{N}_{\text{F}}^{\text{G}}$  state shown in Fig. 4.2 B, an electric field was applied to observe the electrooptic effects. It was found that application of an in-plane field ( $0.1\text{V}/\mu\text{m}$ ) along the rubbing direction for an extended duration ( $>20$  minutes) induces a discontinuous reorientation transition on one surface, irreversibly transitioning the cell into a uniform monodomain with polarization along the field (Fig. 4.3 A-C). When the aligning field is reversed, the  $\text{N}_{\text{F}}^{\text{G}}$

monodomain fails to uniformly reorient, but has small domains reorienting in opposite directions, producing a defect-rich frustrated state (D-F). This state



**Fig. 4.3.** (A) mixture filled in an anti-parallel rubbed cell with  $\pi$  twist state as the ground state. (B, C) Applying  $0.1\text{V}/\mu\text{m}$  in-plane field triggers surface flipping, the mixture in the gap ends up in a homogenous uniform state (D-G) Applying an opposite field force the  $N_F^G$  phase in the gap into a scattering frustration state. (H) Applying the field in the initial orientation unravel the frustration, the phase ends up back in the exact uniform state.

scatters light, becoming more strongly scattering with continued field application, such that the cell becomes turbid for any orientation (G). The process can be fully reversed by reverting to the initial field orientation for  $\sim 10$  mins (H).

A closer look at the turbid state with analyzer out is shown in Fig. 4.4. It appears almost equally dark at all orientations with respect to the polarizer (Fig.

4.4 A-C). This turbid, dark state scatters the transmitted light through it such that no light enters the camera as illustrated in Fig. 4.4 D. Therefore, we call it scattering state and it is transient as it eventually unravels.

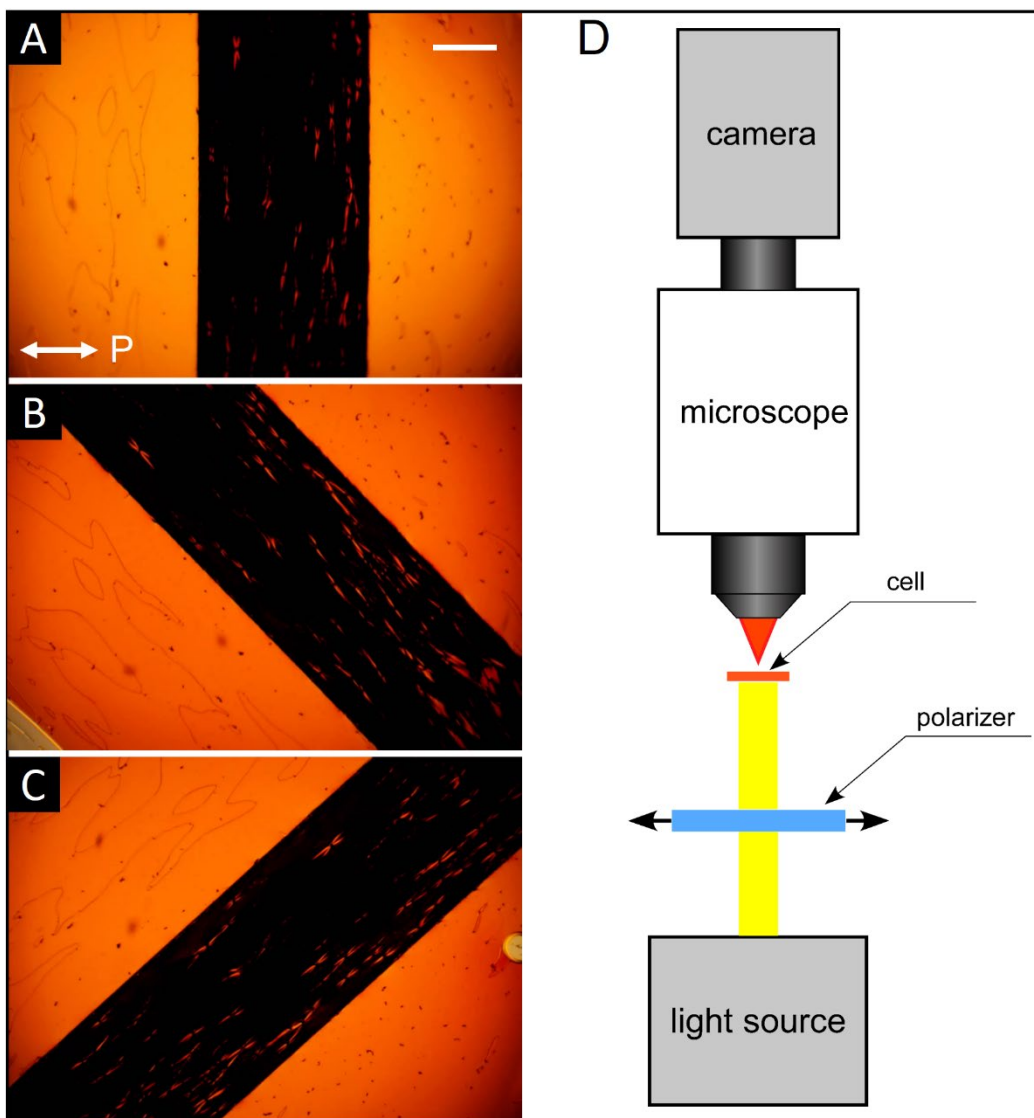


Fig. 4.4. Transient scattering state. (A-C) Images of transient scattering state at different orientations with no analyzer. The scattering state does not depend on the orientation of the polarizer. (D) Schematic sketch of the light path. (Scale bar, 500  $\mu\text{m}$ )

### 4.3 Formation and Annealing of Transient Light Scattering State

To understand the formation and annealing of the transient light scattering state, experiments were repeated with the re-quenched cell. Experiments were

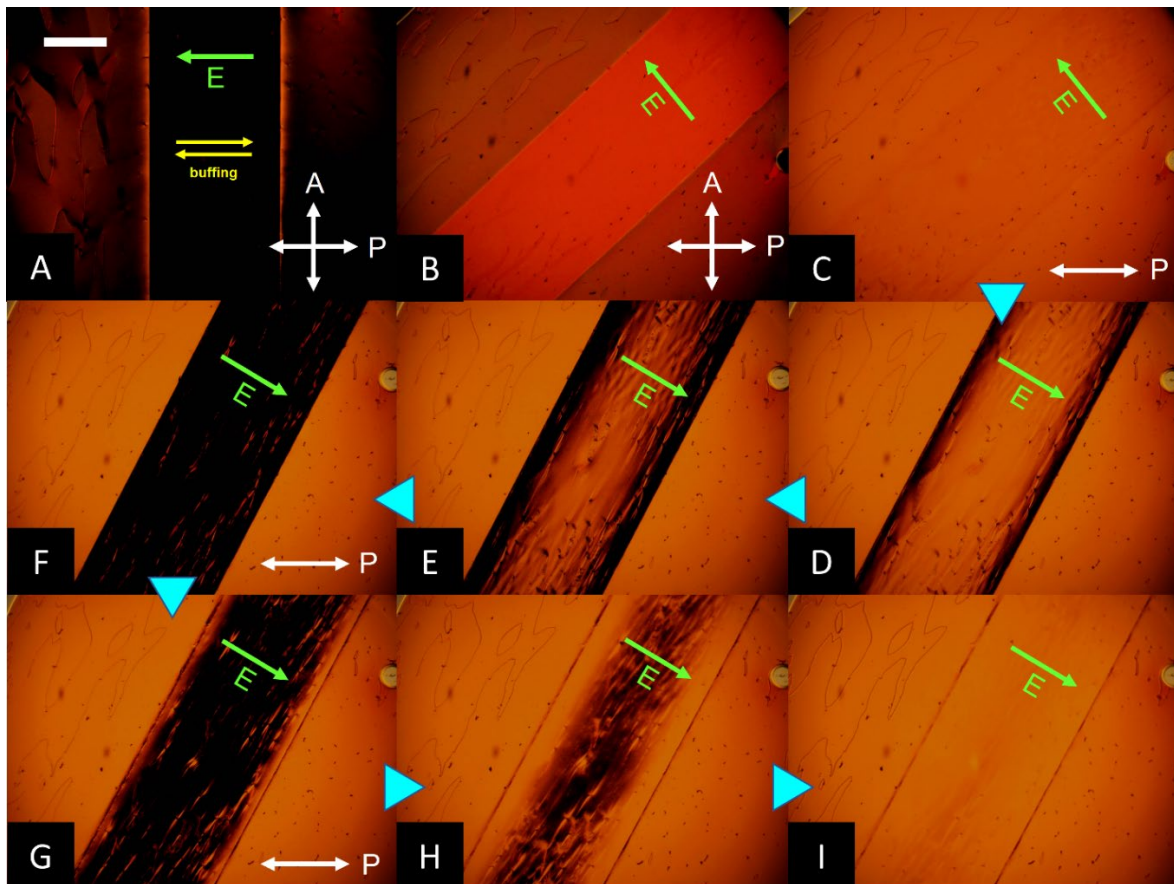


Fig. 4.5. Evolution of the scattering state in a planar-aligned cell of doped RM734 in the  $N_F$  phase ( $t = 8 \mu\text{m}$ ). (A-B) Images taken under crossed analyzer **A** and polarizer **P**. (C-I) Images taken without analyzer **A**. (A-C) Uniformly aligned state after applying  $0.1\text{V/mm}$  for 20 min. The green arrow is the direction of the E-field. (D-I) Growth and disappearance of the scattering state after field reversal. The scattering state is dark with no analyzer. It grows from the electrodes and covers the electrode gap after  $\sim 10$  min. Then annealing starts at the electrodes and is complete after  $\sim 10$  min. (Scale bar,  $500 \mu\text{m}$ .)

conducted at room temperature and the cell was placed on the rotation stage of a polarized light microscope.

The cell was observed in transmission between polarizer and analyzer. The mixture forms a high-viscosity, glassy ferroelectric nematic ( $N_F^G$ ) after quenching to room temperature and forming a  $\pi$  twist state due to the anti-parallel rubbing.

Despite the high viscosity at room temperature, the  $N_F^G$  state could orient homogeneously in an external field. A 0.1V/mm in-plane E-field was applied across the electrode gap, and polarization started to align with the field at a slow rate due to the high rotational viscosity. After 20 mins, a discontinuous reorientation transition was induced on one surface transitioning the cell to a uniform monodomain with polarization along the field. This was confirmed by examining the cell under crossed polarizer and analyzer. The cell was totally extinguished when the director was parallel to the polarizer or the analyzer, Fig. 4.5 (A). It was also uniform at 45° with and without analyzer, Fig. 4.5 (B-C). The aligning field was then reversed as shown in Fig. 4.5 (D) and the  $N_F^G$  monodomain failed to reorient uniformly, but rather formed many small local domains reorienting in opposite directions producing a defect-rich frustrated state, Fig. 4.5 (F). This state was a light scattering state that looked turbid in all directions under crossed polarizer and analyzer, and it was also turbid without analyzer. This frustrated state first grew from the edges of the electrode and slowly covered the entire region between electrodes in 10 mins, Fig. 4.5 (D-F). After another 10 mins, the local domains were

slowly annealed by the in-plane field and the cell returned to a uniform

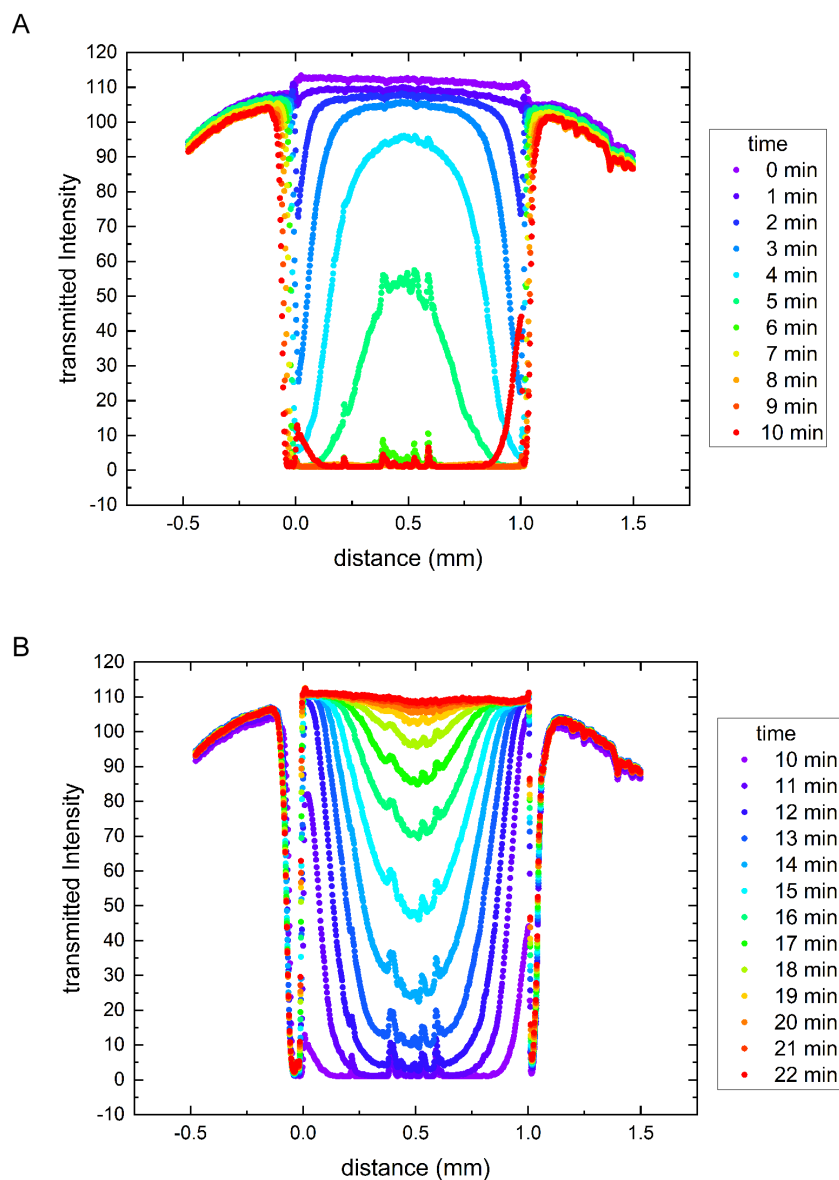


Fig. 4.6. Transmitted intensity across the electrode gap after field reversal. (A) Growth of the scattering state. The in-plane E-field is reversed at  $t = 0$  min. From  $t = 0$  to  $t = 9$  min, transmitted intensity across the entire gap decreases in general to a minimum. The transmitted intensity at edges decreases first followed by that in the middle region producing a front of the scattering state progressing from edges to the middle region. At  $t = 9$  min, the scattering state covers the entire gap, at  $t = 10$  min, transmitted intensity increases at the edges. (B) Disappearance of the scattering state. From  $t = 10$  min to  $t = 22$  min, the transmitted intensity across the gap increases on average back to its maximum

monodomain with polarization along the reversed field, Fig. 4.5 (G-I).

To analyze quantitatively the dynamics of the scattering state, intensity were scanned and processed with MATLAB (Appendix I). The transmitted intensity scans across the electrode gap during the growth and anneal of the scattering states are shown in Fig. 4.6 At  $t = 0$  min, field is just reversed, and the cell is an aligned monodomain. The transmitted intensity is high and uniform along the gap at  $t = 0$  min (Fig. 4 A). It then decays drastically near electrodes and the intensity across the entire gap eventually drops to the minimum at  $t = 10$  mins indicating the growth of the scattering state (Fig. 3 A). From  $t = 10$  mins, the transmitted intensity rebounds as the scattering state disappears (Fig. 3 B). Starting at the electrodes, the transmitted intensity increases and eventually returns to the initial value at  $t = 22$  mins indicating the anneal of the scattering state (Fig. 4 B). The scattering state grows and anneals both start near the electrode gap. The further away from the electrode, the later the scattering state forms or disappears. The difference on the rate of formation and anneal of the scattering state could be resulted from the non-uniform field strength across the gap. The field strength is stronger near the electrode resulting faster reorientation of the LC molecules in the cell.

The dependence of the reversal dynamics on the strength of the reversed E-field is further studied by repeating experiments several times with different reversal field strength applied. In all experiments, the cell was first aligned into a uniform monodomain with polarization along the field by applying a 0.1 V/mm field

for 20 mins. Then the field was reversed and adjusted to different magnitudes in the range of 0.01-0.1V/mm. The lower the magnitude of the reversal field, the longer it took for the scattering state to form. The sizes of the scattering domains also varied with different strengths of field, the smaller the field, the larger the size of local domains. When the reversal field is very small, for example, 0.01 V/mm field was applied, the resulting state is patches of uniform monodomain and stripes of frustrated state.

#### **4.4 Intensity measurements using He-Ne Laser**

To get a quantitative analysis of the dynamics, experiments with the aid of He-Ne laser set-up were performed. The quenched cell was aligned and fixed with a holder such that the laser beam shines on the surface in a normal angle. A photodetector was placed behind the cell on the other side of the laser source to collect the optical signal of the transmitted light. The optical signal is displayed on an oscilloscope. The cell was aligned with the laser set-up in such a way that the laser beam passes through roughly the midpoint of the electrode gap of the cell. A function generator and amplifier were used to apply a 100 V DC field across the electrode gap of the cell. The field was left on for one hour so that the cell was aligned to a uniform monodomain. After the optical signal stops growing and becomes flat, the electric field applied was reversed. First time, the reversed field was 100 V DC. The experiment was repeated with decreased reversal field of 80 V DC and 50 V DC.

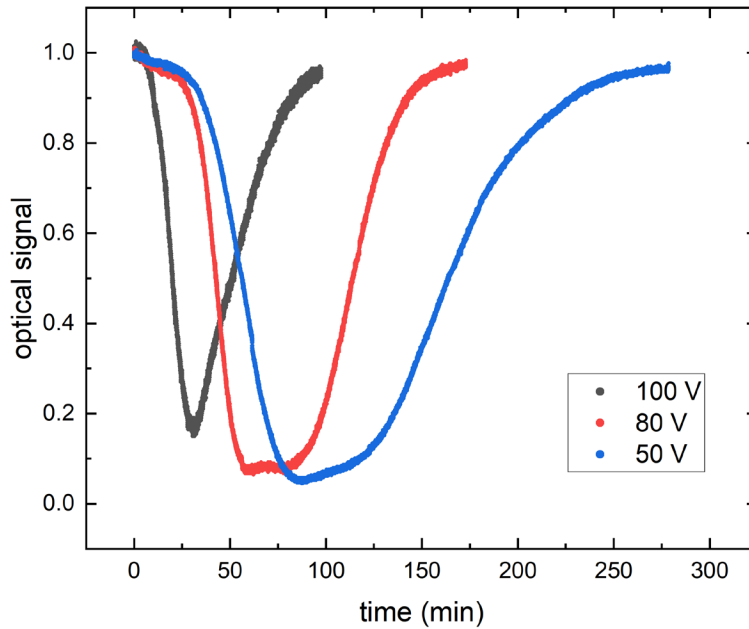
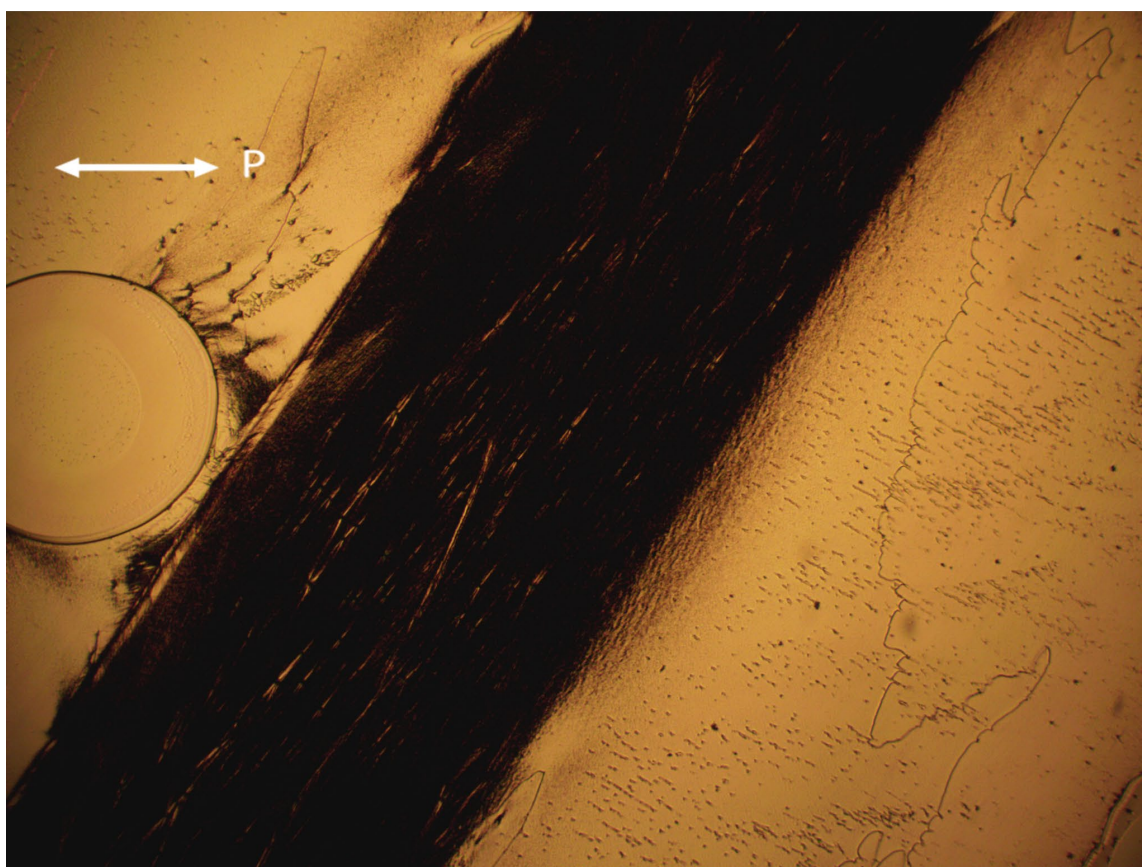
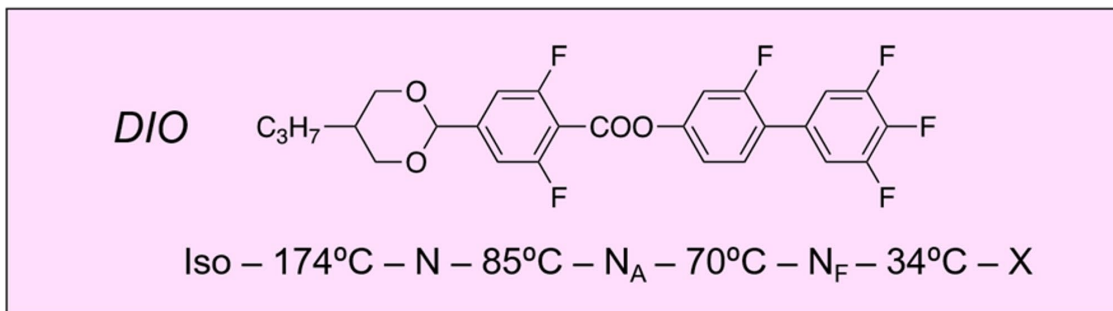


Fig. 4.7. Optical signal of transmitted laser beam detected by photodetector. At  $t=0$  min, applied field is reversed. The black points represent the optical signal detected when reversal field is set to 100 V, where the optical signal decreases/increases with fastest rate and increases immediately after reaching its minimum. The red points represent that of 80 V reversal field, where the optical signal decreases/increases with slightly slower rate, and it stays at its minimum for another 20 mins before rising back to its original level. The blue points are that of 50 V. In this case, the optical signal took more than one hour to decrease to its minimum. It then stays at its minimum for another 50 mins before taking another 150 mins to increase back to its original value.

#### 4.5 Transient Light Scattering State Observed in other $N_F$ with no Dye

To find out whether scattering state is unique to dye-doped  $N_F$ , other cells with mixtures of  $N_F$  phase without dye were also quenched and investigated. Among many mixtures, a sample of 20 wt.% DIO and 80 wt.% RM734 also exhibits transient light-scattering state in reversal field as shown in Fig. 4.8. DIO is another LC material that was found to exhibit  $N_F$  phase [10]. However, the transient light

scattering state in this mixture does not stay too long. It anneals withing 5 mins under 100 V field and crystalized withing 10 mins even with E-field off.



20 wt% DIO and 80 wt% RM734

Fig. 4.8. Molecular structure of DIO[10] and image of scattering state of mixture of 20 wt.% DIO and 80 wt.% RM734 under polarized microscope.

## Chapter 5

### Discussions

This chapter introduces further analysis and findings based on the results presented in the previous chapter. Findings include the dependence of dynamics on temperature and field strength. At last, a model is proposed to explain the dynamics of the transient light-scattering state seen in  $N_F^G$  phase of doped RM734.

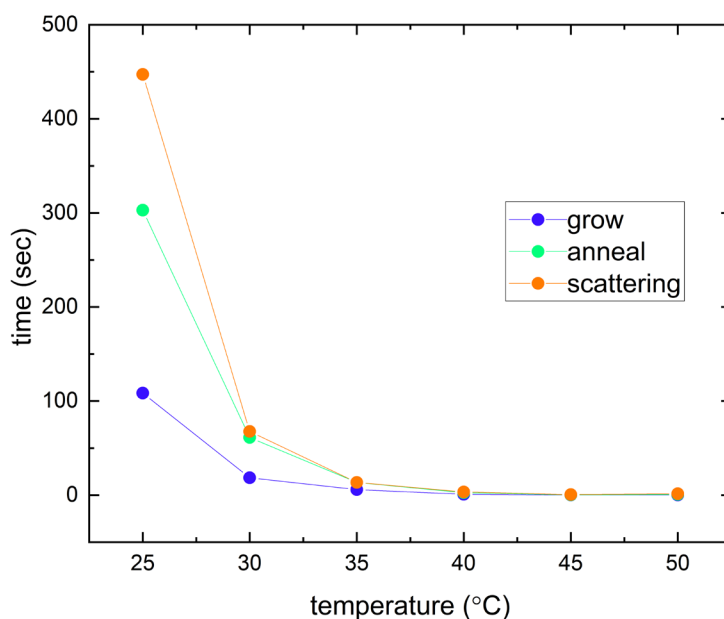


Fig. 5.1 Time durations of processes of the scattering state at different temperatures. The blue points show the time taken for the scattering state to grow such that the intensity of the transmitted light across the cell reduces to one-tenth of the starting value. The green points show the time taken for the scattering state to anneal such that the transmitted intensity across the cell increases from one-tenth of the maximum to the maximum value. The time duration between the process of growing and annealing of the scattering state is represented by the orange dots. From 25 to 50°C, all three processes take less and less time with increase in temperature.

## **5.1 Dependence of the Reversal Dynamics on Temperature**

Experiments were also repeated at different temperatures. From 25 to 50°C, we increased 5°C at a time, each increase in temperature resulted in significant increase in rate of reorientation of the polarization. The time durations taken for the scattering state to grow and to anneal at different temperatures are shown in Fig. 5.1. The data points in Fig. 5.1. are processed from intensities at the midpoint of the cell. A similar pattern is observed near the edge (Appendix II). At 25°C, it takes 2 mins for the scattering state to grow and 5 mins to anneal. The cell remains in the scattering state for more than 7 mins. As the temperature increases, all these dynamics happen faster. At 50°C, it only takes less than 10 secs for all these processes of growing, annealing and scattering state. Similar trends are also observed near the electrodes.

## **5.2 Dependence of the Reversal Dynamics on Field Strength**

From the intensity scan across the gap throughout the process of field reversal in Fig. 4.6, we noticed that the speed at which the scattering state forms/anneals positively proportional to the strength of the field. The scattering state forms/anneals the faster near the electrodes where the field is stronger. This is further confirmed by the laser experiments where changes of optical signal were recorded with different reversal field: 50 V, 80 V and 100 V. The optical signal drops and increases the fastest at 100 V (Fig. 4.7). Dynamics take place slower at 80 V and slowest at 50 V.

### 5.3 Model

In 1991, MacLennan and Clark [2] reported thermal fluctuation effects resulting light scattering from a transient domain-wall. Adopting his analysis, we propose the following 2-D model (Fig. 5.2) to explain the formation of the transient light-scattering state in the glassy ferroelectric nematic mixture at room temperature. Initially, the cell is aligned into a uniform monodomain after applying a strong in-plane DC voltage across the electrode gap for 20 mins due to its ferroelectricity. In this uniform monodomain, molecules all have their polarizations,  $\mathbf{P}$ , aligned with the in-plane field  $\mathbf{E}$  (Fig. 5.2 a). Then the E-field is abruptly reversed. Molecules experience zero torque initially as the angle between  $\mathbf{P}$  and  $\mathbf{E}$  is zero. However, these molecules are not perfectly still due to thermal fluctuations. Molecules wiggle around and eventually start to reorientate, some in clockwise and some in counterclockwise (Fig. 5.2 b). As they rotate in random directions,  $2\pi$  walls are generated between molecules and these  $2\pi$  walls scatter the transmitted light (Fig. 5.2 c-d). Molecules continue to reorient due to the in-plane E-field, and  $2\pi$  walls slowly anneals resulting the disappearance of the scattering state (Fig. 5.2 e-f).

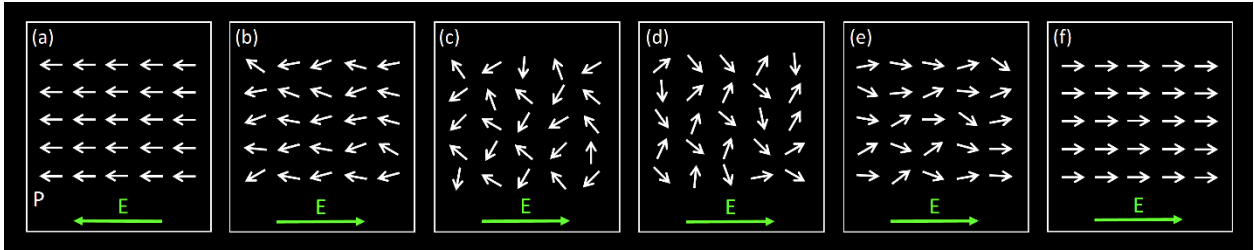


Fig. 5.2. Polarization reorientation response to applied E field. (a) Molecules are aligned with the E-field after applying the 100V DC for 20 min. (b) Direction of E field is reversed causing initial zero torque, but molecules reorient in both clockwise and counterclockwise directions after a while due to thermal fluctuations. (c-d)  $2\pi$  walls that scatter the transmitted light are generated. (e-f)  $2\pi$  walls are annealed and molecules realign with the E field.

In our model, viscosity and strength of the E-field determine the speed at which the scattering state forms and anneals. The lower the viscosity, the faster the molecules reorient. At higher temperature, the rotational viscosity of the mixture drops, and results in shorter duration of the dynamics of the scattering state. The stronger the E-field, the larger the torque experienced by molecules. Molecules reorient faster at stronger E-field resulting in faster dynamics near the electrodes and at higher voltages.

## Chapter 6

### Conclusion

To study and explore the possible electrooptic responses of the recently discovered phase  $N_F$ , samples of  $N_F$  material RM734 and a strong red dye (DR1) were prepared and investigated. In the process of characterizing a particular mixture of 5 wt.% DR1 and 95 wt.% RM734, we found a glassy ferroelectric nematic  $N_F^G$  at room temperature.

Furthermore, the  $N_F^G$  exhibits polar switching in time scales of tens of minutes. The high rotational viscosity of  $N_F^G$  phase in this doped RM734 enabled the generation of uniform polar monodomain that has surface anchoring flipped after the application of a strong DC field. Reversal of the DC field generates  $2\pi$  domain walls that scatter the transmitted light resulting in the formation of the transient light-scattering state in  $N_F^G$  phase observed during the experiments.

The discovery and characterization of the transient light scattering state in  $N_F^G$  phase helps us to better understand the interactions between molecules and E-field.

## References

- [1] X. Chen et al., First-Principles Experimental Demonstration of Ferroelectricity in a Thermotropic Nematic Liquid Crystal: Polar Domains and Striking Electro-Optics, *Proc. Natl. Acad. Sci.* **117**, 14021 (2020).
- [2] J. E. Maclennan and N. A. Clark, Thermal Fluctuation Effects in Ferroelectric Liquid-Crystal Polarization Reversal: Light Scattering from a Transient Domain-Wall Foam, *Phys. Rev. A* **44**, 2543 (1991).
- [3] X. Chen, E. Korblova, M. A. Glaser, J. E. Maclennan, D. M. Walba, and N. A. Clark, Polar In-Plane Surface Orientation of a Ferroelectric Nematic Liquid Crystal: Polar Monodomains and Twisted State Electro-Optics, *Proc. Natl. Acad. Sci.* **118**, e2104092118 (2021).
- [4] I. Dierking, Introduction, in *Textures of Liquid Crystals* (John Wiley & Sons, Ltd, 2003), pp. 1–20.
- [5] D. Demus and R. Lothar, The Structures of Thermotropic Liquid Crystals, in *Textures of Liquid Crystals*, 1st ed. (n.d.).
- [6] P. Oswald and P. Pieranski, *Nematic and Cholesteric Liquid Crystals: Concepts and Physical Properties Illustrated by Experiments*, 0 ed. (CRC Press, 2005).
- [7] S. Lagerwall, Polar Materials and Effects, in *Ferroelectric and Antiferroelectric Liquid Crystals* (John Wiley & Sons, Ltd, 1999), pp. 7–55.
- [8] I. Dierking, Polarizing Microscopy, in *Textures of Liquid Crystals* (2003), pp. 33–42.
- [9] B. Jérôme, Physical Properties: Surface Alignment, in *Handbook of Liquid Crystals* (John Wiley & Sons, Ltd, 1998), pp. 535–548.
- [10] H. Nishikawa, K. Shiroshita, H. Higuchi, Y. Okumura, Y. Haseba, S. Yamamoto, K. Sago, and H. Kikuchi, A Fluid Liquid-Crystal Material with Highly Polar Order, *Adv. Mater.* **29**, 1702354 (2017).

## Appendix I

**MATLAB code for intensity scan across the gap using snapshots from DTLM video:**

First define the vertices of rectangle within which you want to average the intensity,

```
y1 = 700;  
y2 = 2000;  
x1 = 900;  
x2 = 1700;  
B=1;
```

Create empty arrays where you are going to store RGB values read from the snapshot,

```
data=zeros(1301,144);  
data2=zeros(259,418);  
column=1;
```

Standardize the prefix when looping through the folder of snapshots,

```
for i = 1:144  
    if i<2  
        pre = '0000';  
    elseif i<3  
        pre='000';  
    elseif i<18  
        pre='00';  
    else  
        pre='0';  
    end
```

Read RGB values of images,

```
A = imread(strcat("D:\liquid crystal\extracted frames\30C (2s  
interval)\",pre,num2str(B),".png"));
```

Rotate the picture so that the electrode is vertical,

```
vertical = imrotate(A,26);  
red = vertical(x1:x2,y1:y2,1);  
green = vertical(x1:x2,y1:y2,2);  
blue = vertical(x1:x2,y1:y2,3);  
red2 = vertical(x1:x2,498:915,1);  
green2 = vertical(x1:x2,498:915,2);  
blue2 = vertical(x1:x2,498:915,3);
```

Convert RGB values to greyscale using the following function

```
grayscale = 0.2126*red+0.7125*green+0.0772*blue;  
grayscale2=0.2126*red2+0.7125*green2+0.0772*blue2;
```

Take average of grayscale of pixels along vertical direction.

```
average = mean (grayscale);
```

```
average2=mean(grayscale2);
data(:,column)=average;
data2(column,:)=average2;
%surface(vertical(:,1),'LineStyle','none');
%surface(red,'LineStyle','none');
B=B+60;
column=column+1;
end
surface(grayscale(:,1),'LineStyle','none');
M=max(data2,[],"all");
```

## Appendix II

When calculating the rough time durations needed for the scattering state to grow, anneal and remain, relative greyscale values at the midpoint of the cell were used (Fig 5.1). To make sure the data points in the midpoint are representative, the same calculation was made for those at the distance 0.01 mm from the left electrode (Fig 7.1).

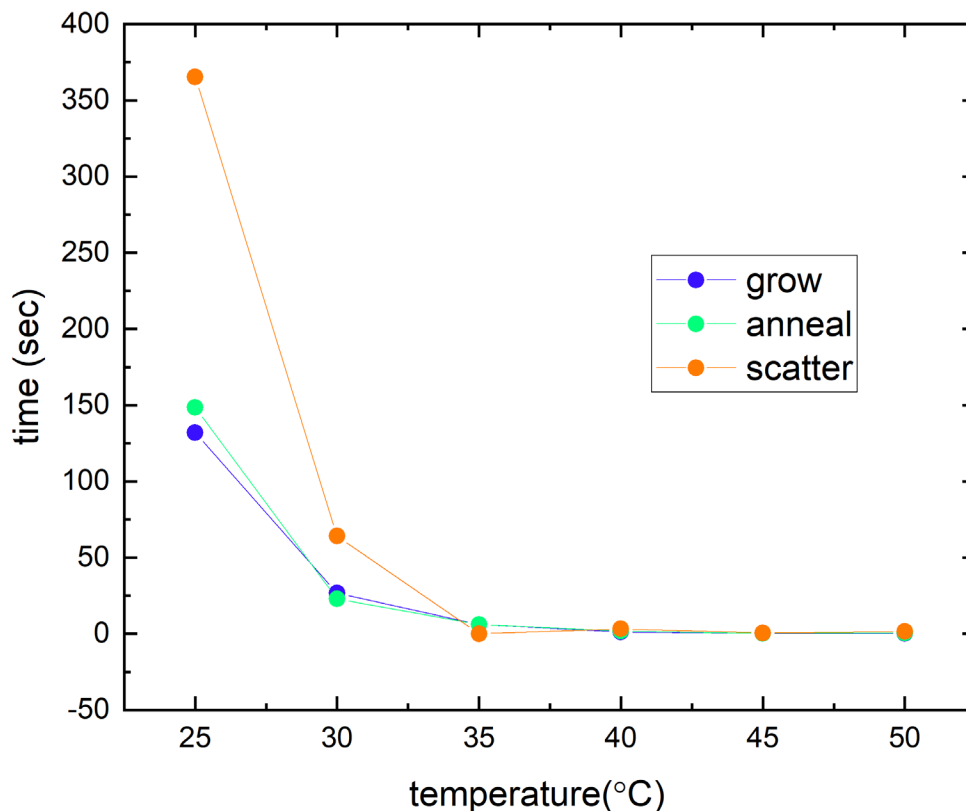


Fig 7.1. Time durations of processes of the scattering state at different temperatures at 0.01 mm right to the left electrode. The blue points show the time taken for the scattering state to grow such that the intensity of the transmitted light across the cell reduces to one-tenth of the starting value. The green points show the time taken for the scattering state to anneal such that the transmitted intensity across the cell increases from one-tenth of the maximum to the maximum